mater.scichina.com link.springer.com

Published online 30 April 2021 | https://doi.org/10.1007/s40843-020-1639-x
Sci China Mater 2021, 64(10): 2430–2438

Ternary organic photodiodes with spectral response from 300 to 1200 nm for spectrometer application

Zhiming Zhong[1,2], Feng Peng[1,2], Lei Ying[1,2*], Gang Yu[1], Fei Huang[1,2] and Yong Cao[1]

ABSTRACT **The light spectrometer is one of the most widely used optical instruments, allowing users to measure and analyze spectral components. However, to reach a broad spectral response range, most spectrometers have to combine a silicon photodiode with an additional photodiode to account for the limited operating wavelength range of each in isolation. Here, we developed organic photodiodes (OPDs) by combining a novel narrow-bandgap non-fullerene acceptor (COTIC-4Cl) with a polymer donor (PCE10) in the presence of $PC_{71}BM$ as the third component. The resulting device based on the ternary blended material showed a wide spectral response from 300 to 1200 nm, beyond the response range of the traditional silicon-based photodiode. Moreover, at the wavelength of 1100 nm, the resulting OPD exhibited a specific detectivity of 5×10^{12} Jones and a responsivity of 0.3 A W^{-1}, with a cut-off frequency of >1 MHz and a linear dynamic range of >120 dB, among the best performances of OPDs. Of particular importance is that, as a proof-of-concept, the resulting ternary OPD was successfully utilized as the key component of a spectrometer to measure the absorption across 300–1200 nm. These results indicate the potential applications of the broadband response OPDs for next-generation spectrometers.**

Keywords: organic photodetector, ternary, non-fullerene acceptor, spectrometer, short-wave infrared

INTRODUCTION

The spectral response range of a photodiode is one of the most critical parameters for its practical application [1–3]. To date, the most widely used photodiodes have been based on a light-sensitive layer of silicon (Si), which typically has a remarkably high detectivity range of 300 to approximately 1000 nm [4]. However, to extend the spectral response range to the short-wave infrared (SWIR) region, spectrometers using Si photodiodes must be further equipped with other photodiodes such as germanium (Ge)- or indium-gallium-arsenide (InGaAs)-based photodiodes [5,6]. This combination raises the complexity of the optical, electrical, and software design and the overall cost of the spectrometer. In this regard, it is highly desirable to develop a single photodiode with a wide spectral response range. Generally, inorganic semiconductors (such as Si, Ge, and InGaAs) feature single-crystal structures, the bandgap of which is determined by the lattice constant. Therefore, it is challenging to integrate them into a single photodiode because of crystal lattice mismatches [7,8]. A viable solution to this issue is to use a light-sensitive layer composed of organic semiconducting materials, which have readily tunable absorption spectra and high extinction coefficients that can achieve broad absorption by blending to form bulk-heterojunction films [9–12].

Recent progress has demonstrated that organic semiconducting materials with strong electron-donating and withdrawing moieties can achieve remarkably high photoresponses in the near-infrared (NIR) and SWIR regions [13–16]. For instance, by incorporating an alkoxyl side chain into the core unit to extend the planarity and intramolecular charge transfer effect, the absorption of the resulting molecule (named IEICO-4F) can be considerably extended to approximately 1000 nm [17]. The organic photodiode (OPD) based on IEICO-4F was developed for the applications in visible and NIR spectral regions [18]. The replacement of the indaceno[1,2-*b*:5,6-*b*′]dithiophene unit with a strong electron-donating core unit of cyclopentadithiophene in combination with rationally designed molecular symmetry produces a small-molecule acceptor (COTIC-4F), the absorption profile of which can be further extended to approximately

[1] Institute of Polymer Optoelectronic Materials and Devices, State Key Laboratory of Luminescent Materials and Devices, South China University of Technology, Guangzhou 510640, China
[2] South China Institute of Collaborative Innovation, Dongguan 523808, China
* Corresponding author (email: msleiying@scut.edu.cn)

1130 nm while maintaining relatively high external quantum efficiency (EQE). However, the dark current density of the OPD based on COTIC-4F was relatively high, thus resulting in a moderate detectivity of about 10^{12} Jones (1 Jones = 1 cm $Hz^{1/2}$ W^{-1}) [19]. These findings testify the great potential of these new organic semiconducting materials as alternative light-sensitive materials relative to their inorganic counterparts, due to their excellent solution-processibility and high extinct coefficients [20].

Herein, we developed a novel non-fullerene acceptor (COTIC-4Cl) containing 2-(5,6-dichloro-3-oxo-2,3-dihydro-1*H*-inden-1-ylidene)malononitrile as the peripheral unit in the CDT-ThOEH group. The slightly stronger dipole moment of *o*-dichlorobenzene (2.77 Debye) than that of *o*-difluorobenzene (2.26 Debye) resulted in a more intense intermolecular charge-transfer [21,22], thus leading to a red-shifted absorption profile that was extended to approximately 1200 nm. The optimized photodiodes based on COTIC-4Cl exhibited a high specific detectivity (D^*) of 5×10^{12} Jones and a responsivity (R) of 0.30 A W^{-1} at 1100 nm, among the best OPDs. These performances, along with response times of <1 μs, a cut-off frequency exceeding 1 MHz, and a large linear dynamic range (LDR) over 120 dB, demonstrated the great potential of this device for practical applications. As a proof-of-concept, we have successfully utilized the fabricated OPD to record the transmittance and absorption of samples from 300 to 1200 nm.

EXPERIMENTAL SECTION

Materials

The PCPDTK-Ph was synthesized according to a previously reported method [23,24], and was dissolved in deionized water (1 mg mL^{-1}). The poly(indenofluorene-co-triphenylamine) (X-IFTPA) was also synthesized according to a previously reported method [25,26], and was dissolved in chlorobenzene (4 mg mL^{-1}). The poly(3,4-ethylenedioxythiophene)-poly(styrenesulfonate) (PEDOT:PSS, PVP AI 4083) was purchased from Heraeus and used as received. The poly[4,8-bis(5-(2-ethylhexyl)thiophen-2-yl)benzo[1,2-b;4,5-b']dithiophene-2,6-diyl-alt-(4-(2-ethylhexyl)-3-fluorothieno[3,4-b]thiophene-)-2-carboxylate-2-6-diyl)] (PCE10) was purchased from ONE Materials Co., Ltd. The COTIC-4Cl was synthesized in our lab (see Scheme S1, ^{1}H nuclear magnetic resonance (NMR) and ^{13}C NMR spectra were illustrated in Figs S1 and S2; the electrochemical and optical properties were list in Table S1). Both $PC_{71}BM$ and C_{60} were purchased from Solenne B. V. The PCE10, COTIC-4Cl and $PC_{71}BM$ were individually dissolved in chlorobenzene (15 mg mL^{-1}) and blended on demand.

OPD fabrication

The indium-tin-oxide (ITO)-coated glass was ultrasonically cleaned by tetrahydrofuran, deionized water, and methanol in sequence. After drying, the substrates were then treated by oxygen plasma (SUNJUNE PLASMA VP-R5) for 1 min prior to the film deposition. A 10-nm-thick PCPDTK-Ph or 30-nm-thick PEDOT:PSS layer was deposited on the top of the substrates, and annealed at 120°C for 10 min to remove residue moisture. The X-IFTPA layer was spin-coated and annealed at 150°C for 20 min. Then the crosslinked films were rinsed with chlorobenzene to remove any non-crosslinked materials. The binary or ternary bulk heterojunction layers with or without 1 vol% 1-chloronaphthalene were prepared. The C_{60}, lithium fluoride (1 nm) and Al (100 nm) layers were deposited in sequence by thermal evaporation at the base pressure of 1×10^{-4} Pa. The device area was 0.0516 cm^2. To fabricate hole- or electron-dominant devices, MoO_3 was used to replace LiF, or PFNBr was used to replace PCPDTK-Ph, respectively. The resulting device configurations were ITO/PCPDTK-Ph/Active layer/MoO_3/Al and ITO/PFNBr/Active layer/LiF/Al, respectively.

Characterization

The absorption and transmittance spectra were scanned by a commercial spectrometer. The EQE and R spectra were measured by a quantum efficiency measurement system with calibrated Si and Ge detectors (Enlitech QE-R3011). The absorption measurement based on OPD was also performed using this setup. In LDR measurement, we used a 1070 nm light-emitting diode (LED) chip (Thorlabs LED 1070E), an InGaAs photodiode (Newport 818-IG/DB) and a source-meter (Keithley 2400). The light intensity was controlled *via* a set of neutral-density filters and the driving current of the LED with the voltage unchanged. As for frequency-dependence measurements, we used a signal generator (Tektronix AFG1062) to drive the 1070 nm LED chip, the output current of the device was amplified by FEMTO DHPCA-100 and then recorded by Tektronix TDS3052B. The noise spectral density characteristics of the OPD were measured by a semiconductor parameter analyzer (Platform Design Automation, Inc. FS380 Pro^{TM}).

RESULTS AND DISCUSSION

Fig. 1a shows the molecular structures of the relevant

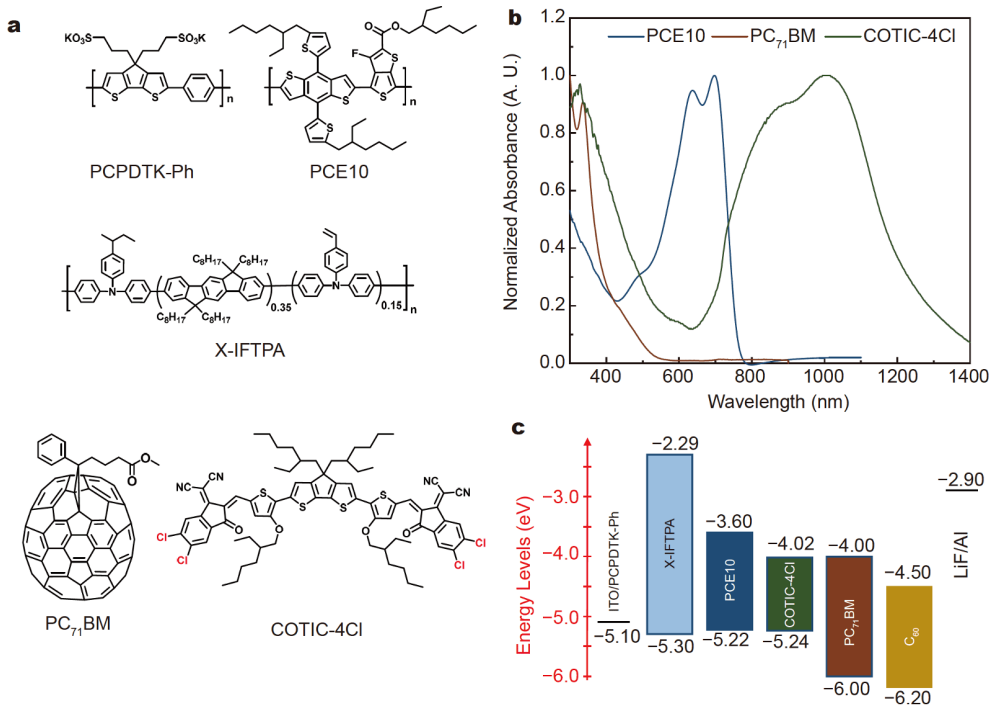

Figure 1 (a) The relevant molecular structures, (b) absorption spectra in film, and (c) energy-level alignment.

materials. The COTIC-4Cl film exhibits broad absorption with a strong absorption band ranging from 600 to about 1400 nm, which is markedly red-shifted relative to its absorption profile in chlorobenzene solution (Fig. S3). Note that the absorption profile of COTIC-4Cl is complementary to that of the electron-donating polymer PCE10, which has a broad absorption band from 300 to 780 nm. Thus, the PCE10:COTIC-4Cl blend film is expected to present a wide range of absorption from approximately 300 to 1200 nm. Moreover, the highest occupied molecular orbital (HOMO) and the lowest unoccupied molecular orbital (LUMO) energy levels of COTIC-4Cl were estimated to be −5.24 and −4.02 eV, respectively. We note that although the LUMO energy level of COTIC-4Cl is much lower than that of −3.60 eV for the polymer donor PCE10, their nearly identical HOMO energy levels may not be able to drive exciton dissociation [27]. To confirm that there would be effective charge separation given such a small difference in the HOMO energy levels, we initially fabricated a device with the structure of ITO/PEDOT:PSS/PCE10:COTIC-4Cl/LiF/Al. Although this device presented only a moderate EQE response upon illumination, its functioning confirmed the effective charge separation. Considering that the widely used PEDOT:PSS shows relatively strong absorbance beyond 900 nm, herein we used an anionic polyelectrolyte, PCPDTK-Ph [23,24], as the interfacial layer to avoid a potential optical loss (Fig. S4). The comparison of the EQE spectra of the devices based on PCPDTK-Ph and PEDOT:PSS demonstrates that the former presents a superior EQE response in the range of 700–1200 nm (Fig. S5).

Introduction of $PC_{71}BM$ as a third component for improved photocurrent

Although we realized a spectral response range from 300 to 1200 nm, we noted that the PCPDTK-Ph-based device exhibited only moderate responsivity (R), which was insufficient for practical applications. To address this issue, we incorporated $PC_{71}BM$ as the third component in the light-sensitive layer, and predicted that it might improve the film morphology in such a way as to facilitate charge transport and thus enhance the responsivity [28–30]. Based on the space-charge-limited current model, the hole/electron mobilities of the device containing PCE10:COTIC-4Cl:$PC_{71}BM$ (with an optimized weight ratio of 9:13:3, Fig. S6) were calculated to be $8.6 \times 10^{-5}/3.7 \times 10^{-6}$ $cm^2\ V^{-1}\ s^{-1}$, which were much higher than those of $1.6 \times 10^{-5}/1.3 \times 10^{-7}$ $cm^2\ V^{-1}\ s^{-1}$ obtained from binary devices containing PCE10:COTIC-4Cl (with an opti-

mized weight ratio of 1:1.5) as the light-sensitive layer (Fig. S7). This observation is consistent with the enhanced EQE of the ternary blended device, which shows a relatively high EQE response exceeding 40% in a broad spectral response range. The presence of $PC_{71}BM$ not only provides cascade energy levels, but also leads to an optimal film morphology. It was reported that a hierarchical morphology can be achieved upon incorporation of $PC_{71}BM$ into the polymer:non-fullerene acceptor system, resulting in an effective charge transport pathway of $PC_{71}BM$ that can facilitate charge transport [30,31]. Note that the EQE reaches 33% at a wavelength of 1100 nm, almost twice the magnitude relative to that of the normal Si-based photodiode (Zolix DSi300, ~17%, Fig. 2). In principle, a device with improved EQE (and R) enables a stronger output signal under the same illumination and pixel size in the spectrometer. It is also worth noting that the NIR-enhanced-type Si photodiode (Hamamatsu S3759) [32], which has an extra-thick light-sensitive layer, only exhibits an R of 0.18 A W^{-1} at 1100 nm. Meanwhile, the R of the optimized ternary OPD at 1100 nm is 0.30 A W^{-1}. As the Si photodiode was specifically developed to detect and measure yttrium aluminum garnet (YAG) lasers at 1060 nm, our device was expected to be capable of the same.

Introduction of charge-blocking layers to suppress dark current

An OPD working in photoconductive mode requires not only a highly efficient conversion of the photon flux to current, but also a low noise current in the dark (J_d). The specific detectivity (D^*) is the figure-of-merit used to describe the signal-to-noise ratio. It has been reported that the charge injection at a reversed bias mainly contributes to the J_d of an OPD [33,34]. Increasing the barrier to charge injection is one of the most effective approaches to dark current suppression, and can be accomplished by incorporating an additional interfacial layer between the organic semiconducting layer and the respective electrode [35,36]. Here, we used a cross-linkable polymer, X-IFTPA, as the anode interfacial layer, because it has a relatively high LUMO energy level of −2.29 eV. Note that X-IFTPA can form a robust film after crosslinking at 150°C for 20 min [25,26]. This film exhibits excellent solvent resistance and enables the sequential deposition of the organic semiconducting layer without damaging the underlying layer. We also incorporated a thin layer of C_{60} as the hole-blocking layer, as this material has a relatively deep HOMO energy level of −6.20 eV (Fig. 1b) [35]. The modified device with the configuration of ITO/PCPDTK-Ph/X-IFTPA/PCE10:COTIC-4Cl:$PC_{71}BM$/C_{60}/LiF/Al has greater charge injection barriers at reversed bias, which is favorable for reducing the J_d. As anticipated, the J_d decreases by two orders of magnitude from 7.1×10^{-6} to 1.1×10^{-8} A cm^{-2} at a reversed bias of −0.1 V after inserting the charge-blocking layers (Fig. 3a), thus confirming that the charge injection under dark conditions can be effectively suppressed. As shown in Fig. 3b, the devices with and without charge-blocking layers exhibit similar spectral responsivity, indicating that the introduction of those layers does not hinder the extraction of photo-generated charge carriers. The slight change in the range of 300–600 nm can be attributed to absorption by X-IFTPA (Fig. S8) and C_{60} in the visible light range. The optimization of thickness is illustrated in Figs S8 and S9. It is interesting to note that the EQE peak contributed by COTIC-4Cl shifted from 900 to 1050 nm as the thickness of active layer decreased from 100 to 60 nm, and the edge became more and more steep, which could be ascribed to the microcavity effect [35].

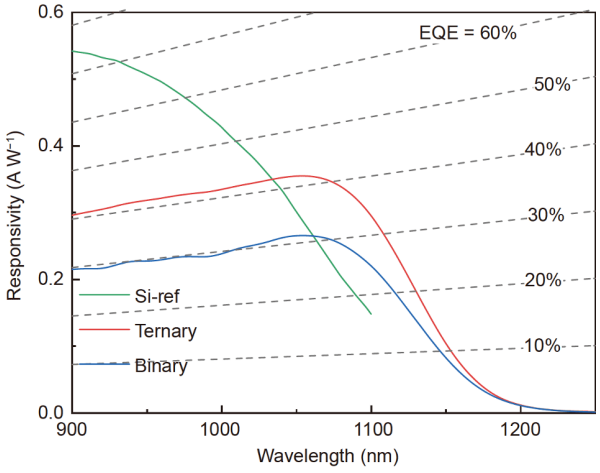

Figure 2 The responsivity characteristics of the binary and ternary OPDs at 0 V with the Si photodiode and EQE contour lines as references.

Note that although the detector is subject to random noise (e.g., shot noise, 1/f noise) [37], the J_d is an average of the measured J over a period. In other words, the peak and valley values of J as a function of time, which are due to the random noise, cancel each other. A separate issue is that the measurement of ultra-low J values could potentially be affected by the parasitic capacity, leading to asymmetry current-voltage (J-V) [33,38]. To further confirm the effect of the charge-blocking layers on device performance, we measured the noise power spectra of the devices with or without charge-blocking layers (Fig. S10). The noise current density of the device with charge-

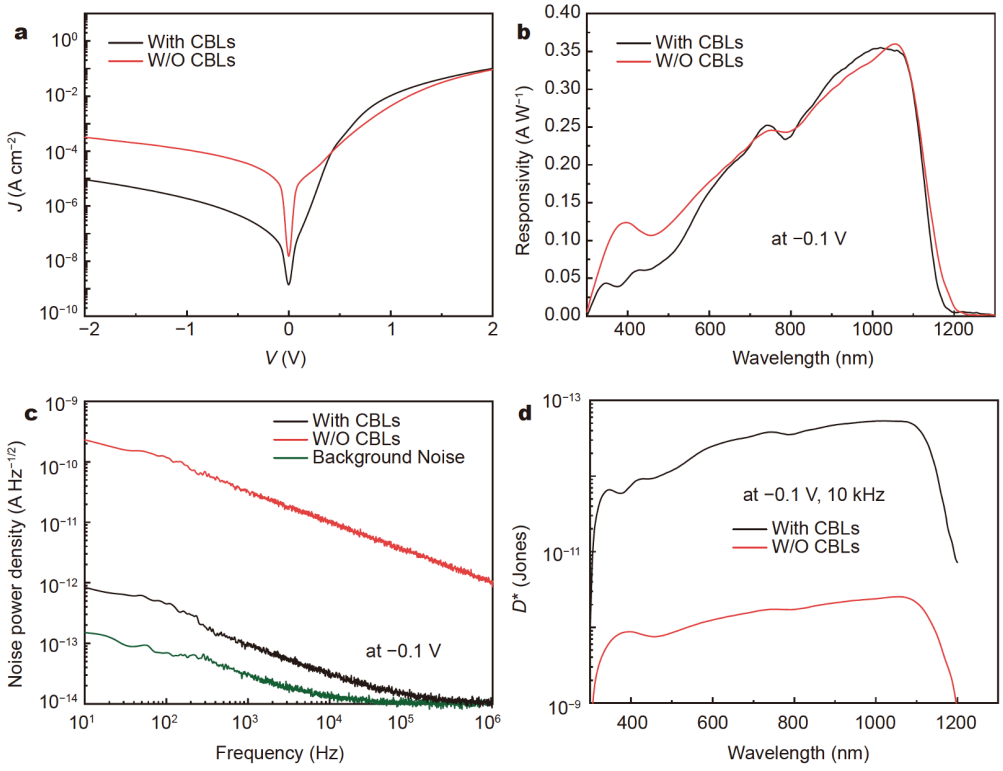

Figure 3 The J_d-V characteristics, (b) noise power density, (c) spectral responsivity, and (d) specific detectivity of OPDs with and without charge-blocking layers (CBLs) at −0.1 V.

blocking layers was measured to be several orders of magnitude smaller than that of the control OPD at a given frequency (Fig. 4b). The specific detectivity can be derived from Equation (1) [39,40]:

$$D^* = \frac{R\sqrt{A}}{i_n}, \quad (1)$$

where i_n is the noise current density, R is the responsivity, and A is the device area (0.0516 cm^2). Therefore, the specific detectivity of the OPD with charge-blocking layers was substantially increased. The D^* at 1100 nm was 5×10^{12} Jones at −0.1 V and 10 kHz, which is better than those of Ge-based (Judson J16, $<2 \times 10^{11}$ Jones at 1100 nm) and InGaAs-based detectors (Hamamatsu G8370-85, $<4 \times 10^{12}$ Jones at 1100 nm) [41,42]. The detailed device performances were summarized in Table S2.

Frequency dependence

Low-speed photodiodes are incapable of sensing a high-frequency or abrupt signal, which causes a distortion in the output signal. The cut-off frequency ($f_{cut\text{-}off}$ or f_{-3db}) is a figure-of-merit used to characterize the frequency dependence and response speed, which is defined as the frequency at which the on/off signal declines to 70.7% (−3 dB) of the original intensity [43]. As shown in Fig. 4a, as the frequency of the input light increased, the output intensity of the OPD became increasingly difficult to maintain. The $f_{cut\text{-}off}$ of our OPD is approximately 1 MHz, which is among the best values for so far reported organic photodiodes [28,43]. At frequencies larger than the $f_{cut\text{-}off}$, the output signal of the OPD was greatly distorted (Fig. S11). In general, the charge carrier is much easier to get rid of trap energy level under strong light illumination. However, in the current case, the $f_{cut\text{-}off}$ of the fabricated OPD remains as high as 2 kHz at an ultra-low light intensity of 40 nW cm^{-2} (Fig. S12), indicating its great promise toward practical applications. When OPDs are applied in cameras, the image may be contaminated by a remnant of the previous frame, if the response times (t_{rise} and t_{drop}) of the image arrays are too slow, leading to a "ghost shadow" in the video picture. However, the t_{rise} and t_{drop} of our device, defined as the times required for the normalized signal intensity to rise from 10% to 90% and drop from 90% to 10%, respectively, are 780 and 940 ns (Fig. 4b), respectively. These values are sufficient

for various applications.

Proof-of-concept for spectrometer applications

The spectrometer is a powerful tool in various research areas. To extend the spectral response beyond 1100 nm, conventional spectrometers containing a Si photodiode must integrate an additional photodiode based on a material such as Ge or InGaAs. This hinders the miniaturization of spectrometers and their integration with other instruments. The emerging low-cost OPDs with highly customizable spectral properties are among the most promising candidates for wide-range spectrometers. Although the OPDs with wide-spectral-response have achieved great progress in recent years, the spectrometer based on them was not reported yet. In this section, we prove that our OPD can be used to measure spectra from 300 to 1200 nm, which is approximately 100 nm beyond the limit of Si-based photodiodes. Assuming that the spectral response was fixed at a given light intensity, i.e., the device had an ideal LDR at each wavelength, the transmittance and absorbance could be measured using the setup in Fig. 5a and calculated according to the following Equations (2) and (3):

$$T = \frac{L_{\text{after}}}{L_{\text{before}}} \times 100\% = \frac{S_{\text{sample}}}{S_{\text{blank}}} \times 100\%, \quad (2)$$

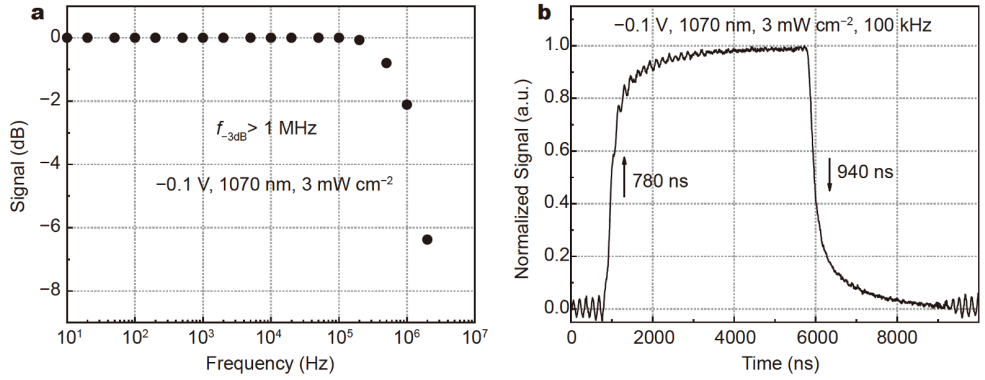

Figure 4 (a) The frequency dependence and (b) response speeds of the optimized OPDs. The raw frequency dependence data are plotted in Fig. S11.

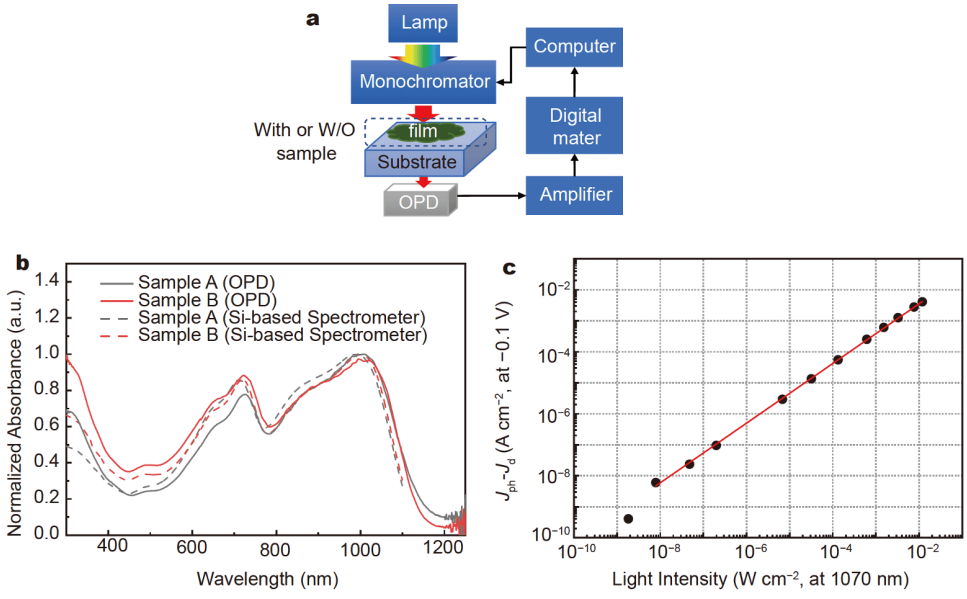

Figure 5 (a) The diagram of the technical setup for absorption measurement by the OPD and the raw data were displayed in Fig. S13. The device structure is ITO/PCPDTK-Ph/X-IFTPA/PCE10:COTIC-4Cl:$PC_{71}BM$=9:13:3 wt./C_{60}/LiF/Al. (b) Comparison of the absorption spectra measured by the OPD and a commercial Si-based spectrometer, the Samples A and B are PCE10:COTIC-4Cl = 1:1.5 (by weight, 190 nm) and PCE10:COTIC-4Cl:$PC_{71}BM$ = 9:13:3 (by weight, 120 nm) in films, respectively. (c) The light-intensity dependence at 1070 nm, −0.1 V, and the fitting equation is $y = 0.3x^{0.963}$, R^2 = 0.99971.

$$A = -\log(T/100\%), \quad (3)$$

where T is the transmittance, S_{sample} is the raw signal of the OPD with the sample as the optical filter, S_{blank} is the raw signal of the OPD without a sample as the optical filter, and the raw signal $S = GI = GRL$, where G is the gain of the current-amplifier, I is the photocurrent, R is the responsivity, which is assumed to be identical before and after the filter, and L is the incident light intensity.

As plotted in Fig. 5b, the normalized absorbance measured by the OPD is almost identical to those measured by a commercial system with Si detectors only, benefiting from the relatively high R across the range of 300–1200 nm and the large LDR. We note that the absorption of the ternary blended PCE10:COTIC-4Cl:$PC_{71}BM$ film showed slightly blue-shifted absorption profile regarding to that of the pure COTIC-4Cl film (Fig. 1b), which might be attributed to the less pronounced aggregation of COTIC-4Cl molecules in the ternary blend film. However, a slight difference can still be noted between the curves measured by our OPD and the commercial system. Besides the differences in the measurement setup (e.g., light source, optical grating and signal amplifier), this discrepancy could be attributed to the light-intensity dependence of the OPD device, implying the need for further calibration and correction. The LDR of our device is >120 dB at 1070 nm, comparable to the LDRs of the InGaAs and Ge photodiodes. Note that in the current case, the maximum light intensity was limited by the power of the light-emitting diode chips. As shown in Fig. 5c, the exponent index is 0.963, which means the photocurrent decayed (or increased) less than the variation of incident light intensity, e.g., the former only decreased to 1/963, when the latter decreased by a factor of 1000. At lower light intensities, OPDs usually yield higher R values (EQE) due to the reduced carrier recombination rates at low concentrations of the photogenerated carriers [27,44]. However, in inorganic semiconductors, the binding energy of excitons is low, and the recombination rate is less affected by the light intensity (the exponent index ~1) [41]. We note that to further improve the spectral accuracy, the light-intensity dependence should be characterized at every wavelength to eliminate discrepancies.

CONCLUSIONS

In summary, we developed an ultra-narrow bandgap acceptor COTIC-4Cl with the absorption spectrum extending to approximately 1200 nm, and constructed OPDs by blending this novel compound with a polymer donor in the presence of $PC_{71}BM$ as a third component. To improve the performance, devices with additional hole- and electron-blocking layers were fabricated to increase the R and suppress the noise current, respectively. As a result, a peak R of 0.35 A W^{-1} and a D^* of >5 × 10^{12} Jones could be achieved at 1050 nm with a bias of −0.1 V. The optimized OPD had a rapid response, with a $t_{rise/fall}$ of 780/940 ns and an $f_{cut\text{-}off}$ exceeding 1 MHz, which are among the best values for any reported OPDs. Compared with a Si-based detector, our OPD had the advantage of a spectral response extended to the wavelength range of 1000–1200 nm. Moreover, our device was successfully used as a key component of a spectrometer to measure the absorption of samples with spectral responses from 300 to 1200 nm. In future, the accuracy of spectrometers based on OPDs could be corrected by using machine learning to compare large numbers of curves measured by the OPD with those obtained by a certified system.

Received 23 December 2020; accepted 5 February 2021; published online 30 April 2021

1 Tan CL, Mohseni H. Emerging technologies for high performance infrared detectors. Nanophotonics, 2018, 7: 169–197
2 Wu Z, Zhai Y, Kim H, *et al.* Emerging design and characterization guidelines for polymer-based infrared photodetectors. Acc Chem Res, 2018, 51: 3144–3153
3 Gong X, Tong M, Xia Y, *et al.* High-detectivity polymer photodetectors with spectral response from 300 nm to 1450 nm. Science, 2009, 325: 1665–1667
4 Huang J, Lee J, Vollbrecht J, *et al.* A high-performance solution-processed organic photodetector for near-infrared sensing. Adv Mater, 2020, 32: 1906027
5 Rogalski A. History of infrared detectors. Opto-Electron Rev, 2012, 20: 279–308
6 Fan D, Lee K, Forrest SR. Flexible thin-film InGaAs photodiode focal plane array. ACS Photonics, 2016, 3: 670–676
7 Michel J, Liu J, Kimerling LC. High-performance Ge-on-Si photodetectors. Nat Photon, 2010, 4: 527–534
8 Chiba K, Yoshida A, Tomioka K, *et al.* Vertical InGaAs nanowire array photodiodes on Si. ACS Photonics, 2019, 6: 260–264
9 Jansen-van Vuuren RD, Armin A, Pandey AK, *et al.* Organic photodiodes: the future of full color detection and image sensing. Adv Mater, 2016, 28: 4766–4802
10 Chow PCY, Someya T. Organic photodetectors for next-generation wearable electronics. Adv Mater, 2020, 32: 1902045
11 Yoon S, Sim KM, Chung DS. Prospects of colour selective organic photodiodes. J Mater Chem C, 2018, 6: 13084–13100
12 Liu J, Wang Y, Wen H, *et al.* Organic photodetectors: materials, structures, and challenges. Sol RRL, 2020, 4: 2000139
13 Li Q, Guo Y, Liu Y. Exploration of near-infrared organic photodetectors. Chem Mater, 2019, 31: 6359–6379
14 Yeddu V, Seo G, Cruciani F, *et al.* Low-band-gap polymer-based infrared-to-visible upconversion organic light-emitting diodes with infrared sensitivity up to 1.1 μm. ACS Photonics, 2019, 6: 2368–

2374
15 Liu X, Lin Y, Liao Y, *et al.* Recent advances in organic near-infrared photodiodes. J Mater Chem C, 2018, 6: 3499–3513
16 Wang C, Zhang X, Hu W. Organic photodiodes and phototransistors toward infrared detection: materials, devices, and applications. Chem Soc Rev, 2020, 49: 653–670
17 Wang J, Xie S, Zhang D, *et al.* Ultra-narrow bandgap non-fullerene organic solar cells with low voltage losses and a large photocurrent. J Mater Chem A, 2018, 6: 19934–19940
18 Huang Z, Zhong Z, Peng F, *et al.* Copper thiocyanate as an anode interfacial layer for efficient near-infrared organic photodetector. ACS Appl Mater Interfaces, 2021, 13: 1027–1034
19 Lee J, Ko SJ, Lee H, *et al.* Side-chain engineering of nonfullerene acceptors for near-infrared organic photodetectors and photovoltaics. ACS Energy Lett, 2019, 4: 1401–1409
20 Fuentes-Hernandez C, Chou WF, Khan TM, *et al.* Large-area low-noise flexible organic photodiodes for detecting faint visible light. Science, 2020, 370: 698–701
21 Zhang H, Yao H, Hou J, *et al.* Over 14% efficiency in organic solar cells enabled by chlorinated nonfullerene small-molecule acceptors. Adv Mater, 2018, 30: 1800613
22 Kini GP, Jeon SJ, Moon DK. Design principles and synergistic effects of chlorination on a conjugated backbone for efficient organic photovoltaics: a critical review. Adv Mater, 2020, 32: 1906175
23 Xie Q, Zhang J, Xu H, *et al.* Self-doped polymer with fluorinated phenylene as hole transport layer for efficient polymer solar cells. Org Electron, 2018, 61: 207–214
24 Kang Q, Liao Q, Xu Y, *et al.* p-Doped conducting polyelectrolyte as an anode interlayer enables high efficiency for 1 cm^2 printed organic solar cells. ACS Appl Mater Interfaces, 2019, 11: 20205–20213
25 Zhong Z, Wang X, Guo T, *et al.* Crosslinkable triphenylamine-based hole-transporting polymers for solution-processed polymer light-emitting diodes. Org Electron, 2018, 53: 35–42
26 Zhong Z, Peng F, Huang Z, *et al.* High-detectivity non-fullerene organic photodetectors enabled by a cross-linkable electron blocking layer. ACS Appl Mater Interfaces, 2020, 12: 45092–45100
27 He Z, Xiao B, Liu F, *et al.* Single-junction polymer solar cells with high efficiency and photovoltage. Nat Photon, 2015, 9: 174–179
28 Li W, Xu Y, Meng X, *et al.* Visible to near-infrared photodetection based on ternary organic heterojunctions. Adv Funct Mater, 2019, 29: 1808948
29 Liu ZX, Lau TK, Zhou G, *et al.* Achieving efficient organic solar cells and broadband photodetectors *via* simple compositional tuning of ternary blends. Nano Energy, 2019, 63: 103807
30 Zhou Z, Xu S, Song J, *et al.* High-efficiency small-molecule ternary solar cells with a hierarchical morphology enabled by synergizing fullerene and non-fullerene acceptors. Nat Energy, 2018, 3: 952–959
31 Li H, Lu K, Wei Z. Polymer/small molecule/fullerene based ternary solar cells. Adv Energy Mater, 2017, 7: 1602540
32 Hamamatsu. Datasheet of S3759. http://www.hamamatsu.com.cn/UserFiles/upload/file/20190710/s3759_kpin1066e.pdf
33 Simone G, Dyson MJ, Weijtens CHL, *et al.* On the origin of dark current in organic photodiodes. Adv Opt Mater, 2020, 8: 1901568
34 Simone G, Dyson MJ, Meskers SCJ, *et al.* Organic photodetectors and their application in large area and flexible image sensors: the Role of dark current. Adv Funct Mater, 2020, 30: 1904205
35 Siegmund B, Mischok A, Benduhn J, *et al.* Organic narrowband near-infrared photodetectors based on intermolecular charge-transfer absorption. Nat Commun, 2017, 8: 15421
36 Li T, Chen Z, Wang Y, *et al.* Materials for interfaces in organic solar cells and photodetectors. ACS Appl Mater Interfaces, 2020, 12: 3301–3326
37 Wu Z, Yao W, London AE, *et al.* Elucidating the detectivity limits in shortwave infrared organic photodiodes. Adv Funct Mater, 2018, 28: 1800391
38 Yokota T, Nakamura T, Kato H, *et al.* A conformable imager for biometric authentication and vital sign measurement. Nat Electron, 2020, 3: 113–121
39 Fang Y, Armin A, Meredith P, *et al.* Accurate characterization of next-generation thin-film photodetectors. Nat Photon, 2018, 13: 1–4
40 Kim IK, Jo JH, Lee JB, *et al.* Detectivity analysis for organic photodetectors. Org Electron, 2018, 57: 89–92
41 Judson. Datasheet of J16. http://www.teledynejudson.com/prods/Documents/Ge_shortform_August2004.pdf
42 Hamamatsu. Datasheet of G8370-85. http://www.hamamatsu.com.cn/UserFiles/upload/file/20190918/g8370-81_etc_kird1064e.pdf
43 Strobel N, Seiberlich M, Rödlmeier T, *et al.* Non-fullerene-based printed organic photodiodes with high responsivity and megahertz detection speed. ACS Appl Mater Interfaces, 2018, 10: 42733–42739
44 Ho JKW, Yin H, So SK. From 33% to 57%—an elevated potential of efficiency limit for indoor photovoltaics. J Mater Chem A, 2020, 8: 1717–1723

Acknowledgements This work was financially supported by the Natural Science Foundation of Guangdong Province (2019B030302007, 2020A1515011028 and 2017A030306011), the National Natural Science Foundation of China (51933003 and 22005102), the Program for Science and Technology Development of Dongguan (2019622163009), and Dongguan Innovative Research Team Program (2018607201002). Zhong Z thanks the financial support from China Postdoctoral Science Foundation (2020M682696).

Author contributions Ying L and Zhong Z designed the experiments; Peng F did the synthesis and characterization of the molecules. Zhong Z carried out the device experiments and wrote the paper with the support from Yu G, Huang F and Cao Y. All authors contributed to the general discussion.

Conflict of interest The authors declare no conflict of interest.

Supplementary information Experimental details and supporting data are available in the online version of the paper.

Zhiming Zhong received his PhD degree from the South China University of Technology in 2017. Now he continues his postdoctoral research at the South China University of Technology with Prof. Yong Cao. He is majored in organic semiconductors and devices, including organic LEDs, organic photodetectors and their applications.

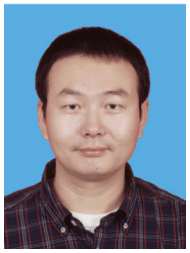

Lei Ying received his PhD degree from the South China University of Technology in 2009. Then he worked at the University of California, Santa Barbara, as a postdoctoral research fellow with Prof. Guillermo C. Bazan. In 2013, he joined the South China University of Technology and was promoted to associate professor. His current interests include developing new organic semiconductors for opto-electronic devices.

光谱响应覆盖300–1200 nm的三元有机光敏二极管及其在光谱仪中的应用

钟知鸣[1,2], 彭洋[1,2], 应磊[1,2*], 俞钢[1], 黄飞[1,2], 曹镛[1]

摘要 光谱仪是科研中应用最广泛的光学仪器之一, 常用于测量和分析光谱成分. 为了实现宽且连续的光谱响应范围, 光谱仪需将多种不同波长响应范围的光敏二极管联合起来使用. 本文中, 我们基于吸收光谱互补的设计思路将一种新型的窄带隙受体(COTIC-4Cl)与聚合物给体(PCE10)相结合, 并引入$PC_{71}BM$作为第三组分, 开发了高性能宽波段的有机光敏二极管(OPD). 基于三元混合的光探测器显示出300至1200 nm的宽光谱响应, 超出了传统硅基光电二极管的响应范围(300–1100 nm). 此外, 在波长1100 nm处, 该器件表现出5×10^{12} Jones的探测率和0.3 A W^{-1}的响应率, 并且截止频率大于1 MHz, 线性动态范围大于120 dB, 是目前报道的OPD中性能最好的器件之一. 为了验证OPD在光谱仪中应用的可行性, 我们将该器件用作光谱仪的关键部件, 可以在300–1200 nm波长范围成功测量样品的吸收光谱. 这些结果预示, 高性能宽波段的OPDs在下一代光谱仪中的应用前景十分广阔.

